Chapter 6: Paleoclimate

Coordinating Lead Authors:
Eystein Jansen, Jonathan Overpeck

Lead Authors:
Keith R. Briffa, Jean-Claude Duplessy, Fortunat Joos, Valérie Masson-Delmotte, Daniel O. Olago, Bette Otto-Bleisner, Wm. Richard Peltier, Stefan Rahmstorf, R. Ramesh, Dominique Raynaud, David H. Rind, Olga Solomina, Ricardo Villalba, De'er Zhang

Contributing Authors:
Jean-Marc Barnola, Mark Chandler, Julia Cole, Trond Dokken, Dominik Fleitmann, Myriam Khodri, Øyvind Lie, Erik Monnin, Daniel Muhs, Tim Osborn, Frederic Parrenin, Henry N. Pollack, Øyvind Paasche, Ellen Mosley-Thompson, Lonnie Thompson, Jim Zachos

Review Editors: Jean Jouzel, John Mitchell

Date of Draft: 12 August 2005

Notes: This is the TSU compiled version.

Figures

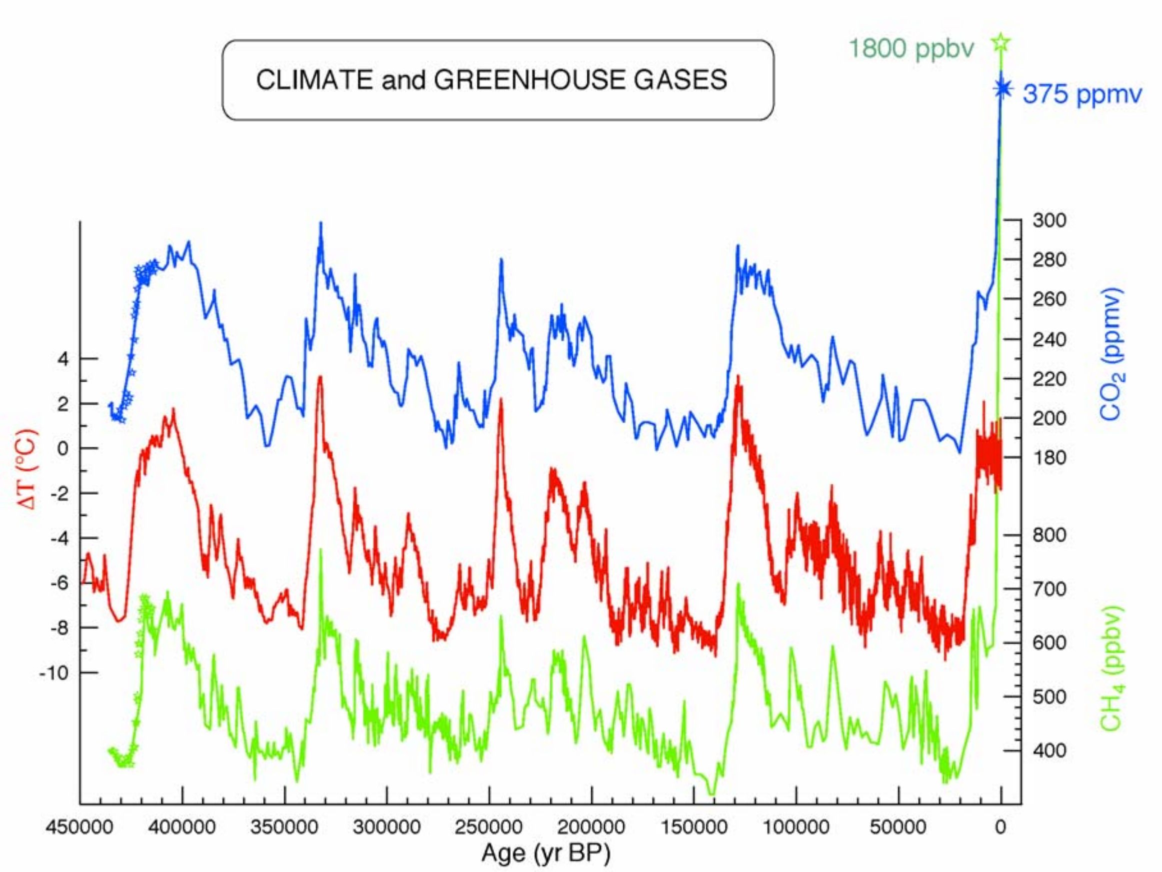

Figure 6.1. The Vostok ice core record covers the last 4 glacial cycles and has recently been extended to obtain a complete record back to 450ka (and through the Marine Isotope Stage 11 Interglacial Period). The figure shows the CO_2 (Petit et al., 1999b; Pépin et al., 2001; Raynaud et al., 2005), CH_4 (Petit et al., 1999b; Delmotte et al., 2004; Raynaud et al., 2005), and deuterium, a proxy scaled here in Antarctic temperature changes from the present, (Petit et al., 1999b) records.The stars plotted before 400ka indicate the CO_2 and CH_4 measurements performed on the independent EPICA DC core for the transition between Stages 12 and 11 (EPICA-COMMUNITY-MEMBERS, 2004); these measurements confirm the fidelity of the Vostok record.

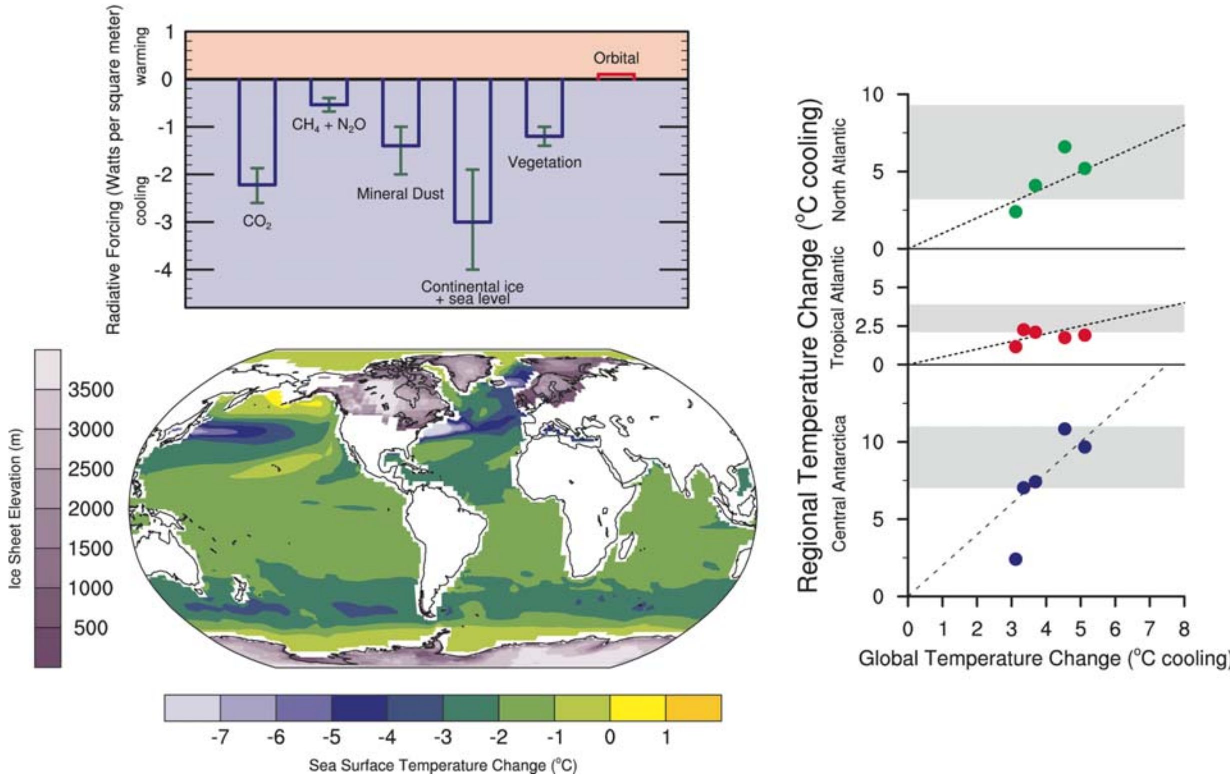

Figure 6.2. Last Glacial Maximum (21,000 years ago) relative to pre-industrial (1750). Top left: Global, annual mean radiative forcings (W/m^2). For detailed explanations see text. The height of the rectangular bars and the uncertainty ranges denote a best estimate values guided by published values of the forcing and physical understanding. All the forcings shown have distinct spatial and seasonal features such that the global annual means do not yield a complete picture of the radiative perturbation. Bottom left: Mean-model SST change for five PMIP-2 models (CCSM3, ECBILT-CLIO, HadCM3M2, IPSL, and MIROC3.2) and ICE-5G ice sheet reconstruction over continents (Peltier, 2004a). Right: Comparison of regional cooling compared to global cooling as simulated by PMIP-2 models, plotted as solid circles. Grey shading indicates range of proxy estimates of regional cooling (Kageyama et al., 2005; Masson-Delmotte et al., 2005; Schneider von Deimling et al., submitted). Dashed lines correspond to slopes of 1 for the North Atlantic, 0.5 for the tropical Atlantic, and 2 for central Antarctica.

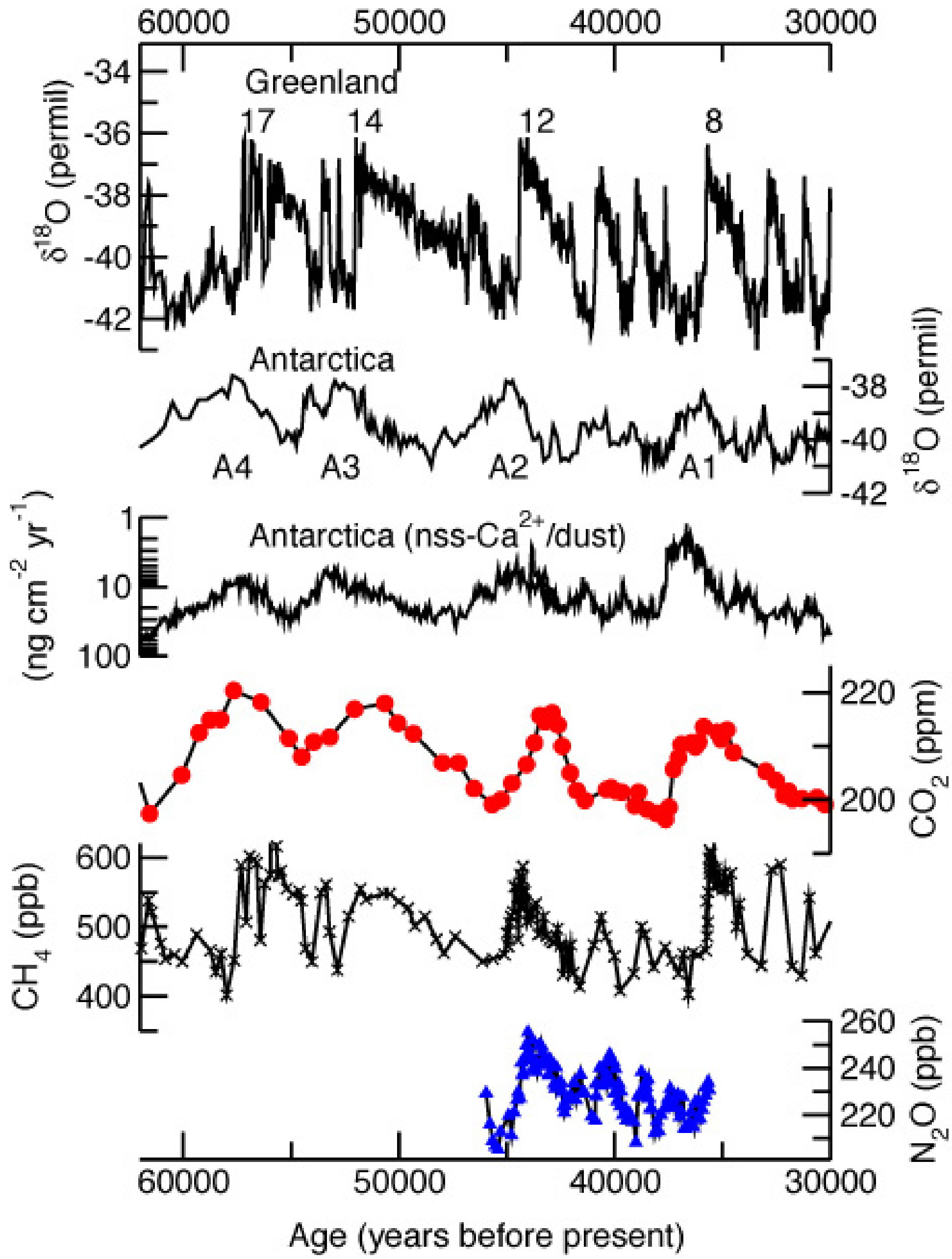

Figure 6.3. The evolution of atmospheric CO_2 concentration and Greenland and Antarctic temperature as indicated by $\delta^{18}O$, during the period from 70 ka BP to 20 ka BP (Indermühle et al., 2000). $\delta^{18}O$ values are from ice drilled at Summit during the Greenland Ice Core Project (GRIP) and Vostok, Antarctica, and CO_2 data are from Taylor Dome, Antarctica. All data are plotted on the GT4 chronology of Vostok. Dansgaard/Oeschger events, the Heinrich events, recorded as ice-rafted debris in marine sediments in the North Atlantic, and the Antarctic warm periods (A4 to A1) are all shown. The GRIP, Vostok, and Taylor Dome ice cores were synchronized based on methane measurements. The location of Heinrich events is based on the synchronization of the GRIP ice core to North Atlantic deep-sea cores (Bond and Lotti, 1995).

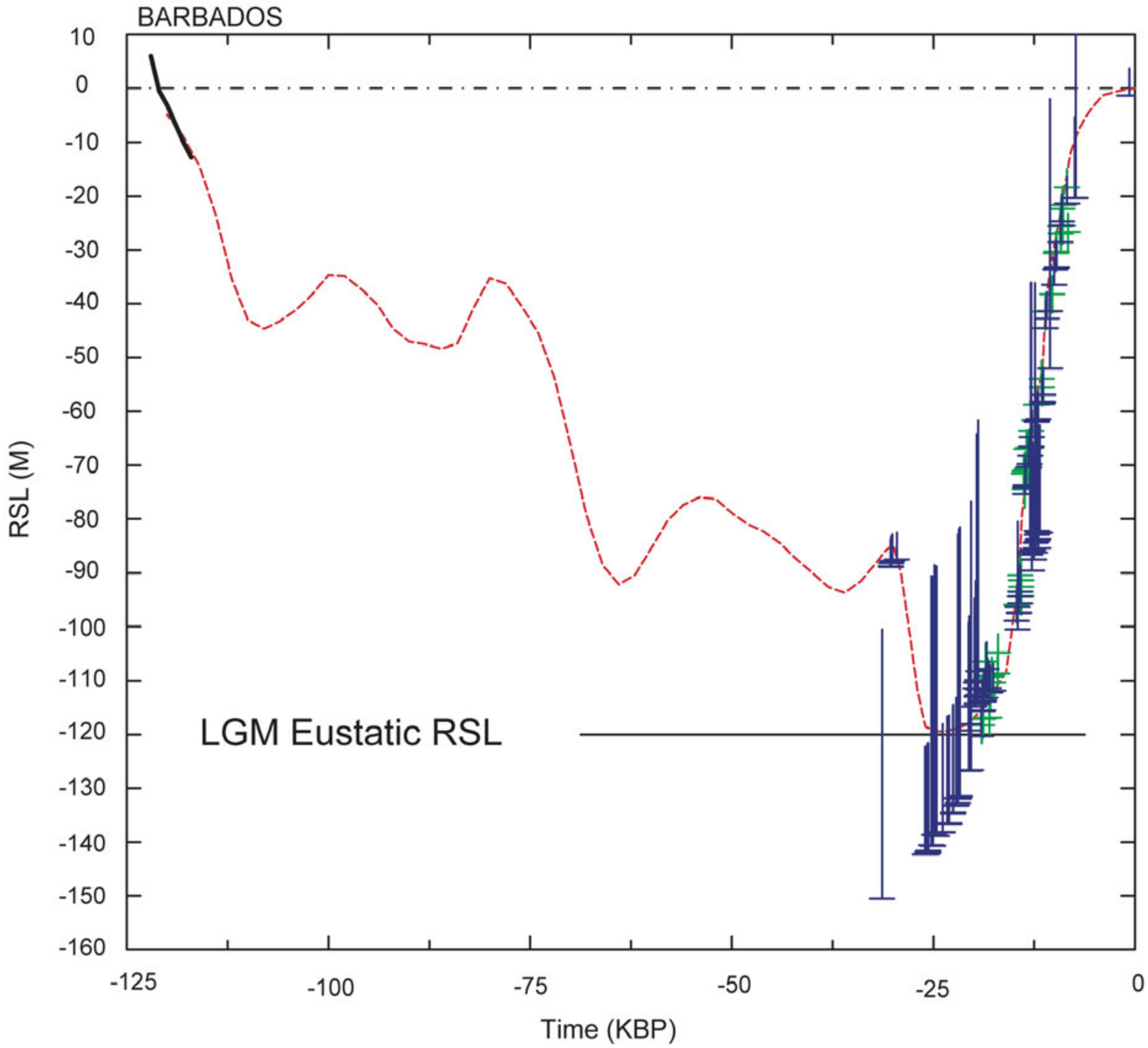

Figure 6.4. The fit of the ICE-5G(VM2) model of the glacial isostatic adjustment process to the coral based record (Fairbanks, 1989) of relative sea level history from the island of Barbados in the Caribbean Sea over the age range from the present day to 30,000 years before present (BP; note: time scale in kyrs BP). The individual coral based estimates of relative sea level are color coded by the species of coral on which the individual estimates are based. The green estimates are derived from the *Acropora Palmata*, which provide the tightest constraints upon relative sea level. The estimates denoted by blue error bars are derived either from the *Monastrea Annularis* species of coral (error bars of intermediate length) or from other species which are found over a wider range of depths with respect to sea level (longest error bars). The sea level curve for the period extending from 30,000 ka back to the LIG centered on 125,000 ka has been constructed by employing the oxygen isotope based SPECMAP record. The data suggest that the eustatic depression of sea level at the LGM was approximately 120m, the number preferred by Shackleton (2000) based solely upon oxygen isotope analysis.

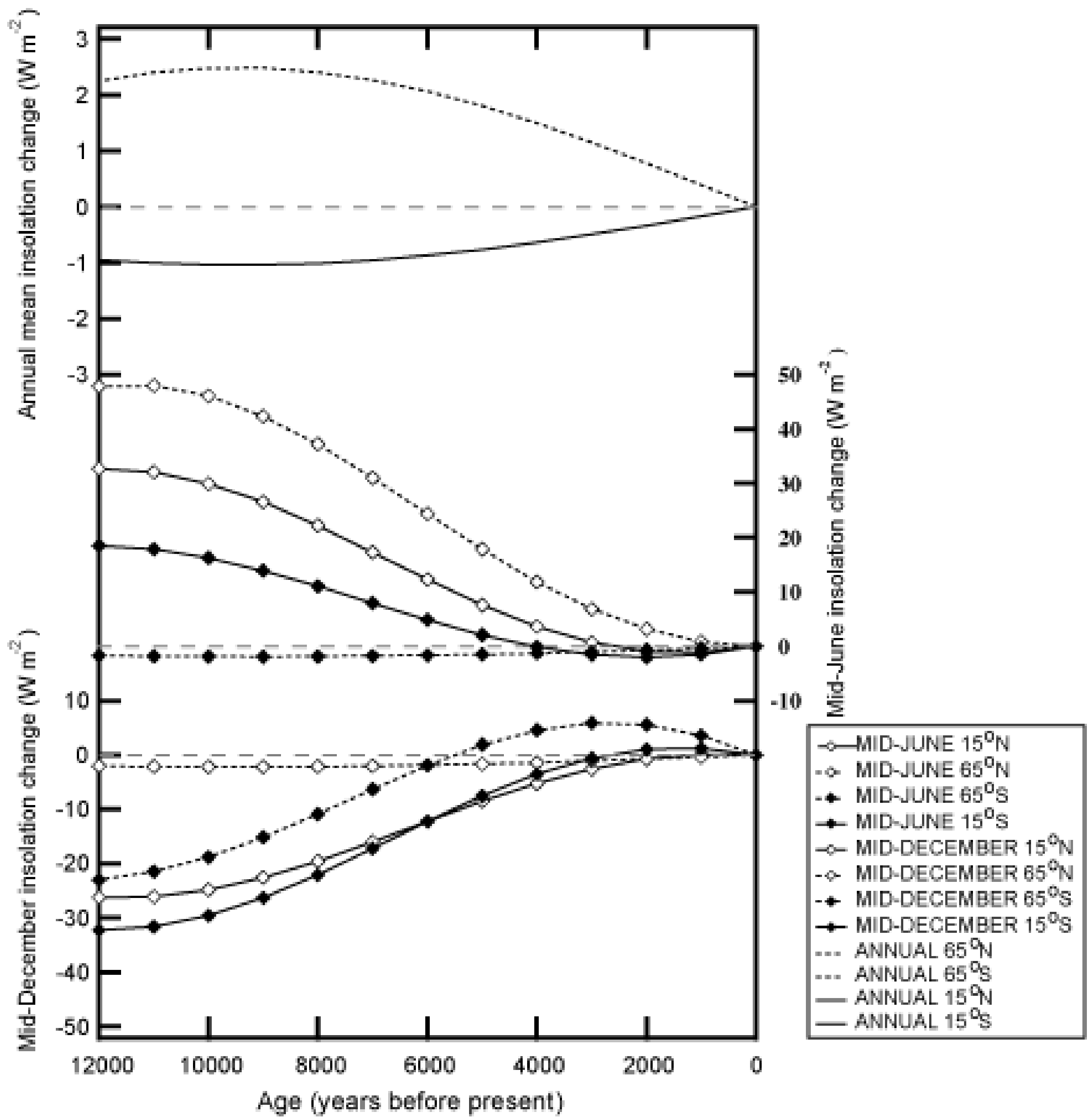

Figure 6.5. Orbital forcing during the current interglacial period (the Holocene). Long-term changes in the Earth's orbit modulate the latitudinal and seasonal distribution of incoming solar radiation, represented here as deviations from the current millennium values, as a function of age (in thousands of years before present, 1950 A.D.) (Berger and Loutre, 1991). Small annual mean insolation changes (top panel, less than 2.5W/m^2) occur with opposite trends at low and high latitudes, in response to changes in the obliquity of the Earth. These changes in obliquity interact with changes in the precession of the equinox to generate one order of magnitude larger (up to ~50 W/m^2) changes in the seasonal cycle of incoming solar radiation, here represented by mid-June (mid panel) and mid-January (bottom panel) daily insolation changes.

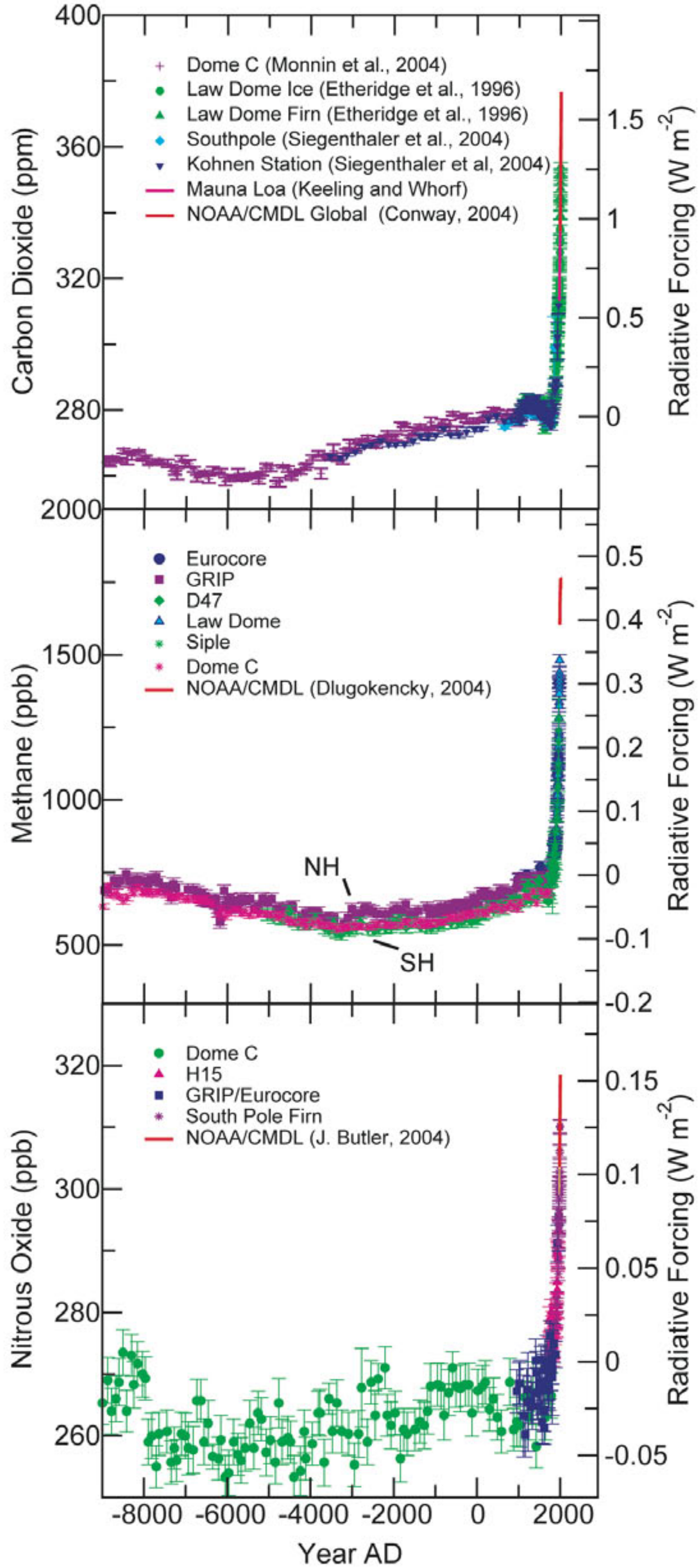

Figure 6.6. Observed changes in atmospheric greenhouse gas composition during the current interglacial period (as a function of years A.D.). a) Carbon dioxide; b) Methane; c) Nitrous oxide. Superimposed on ice-core based reconstructions are displayed direct firn sampling and contemporary instrumental measurements (pink and red lines).

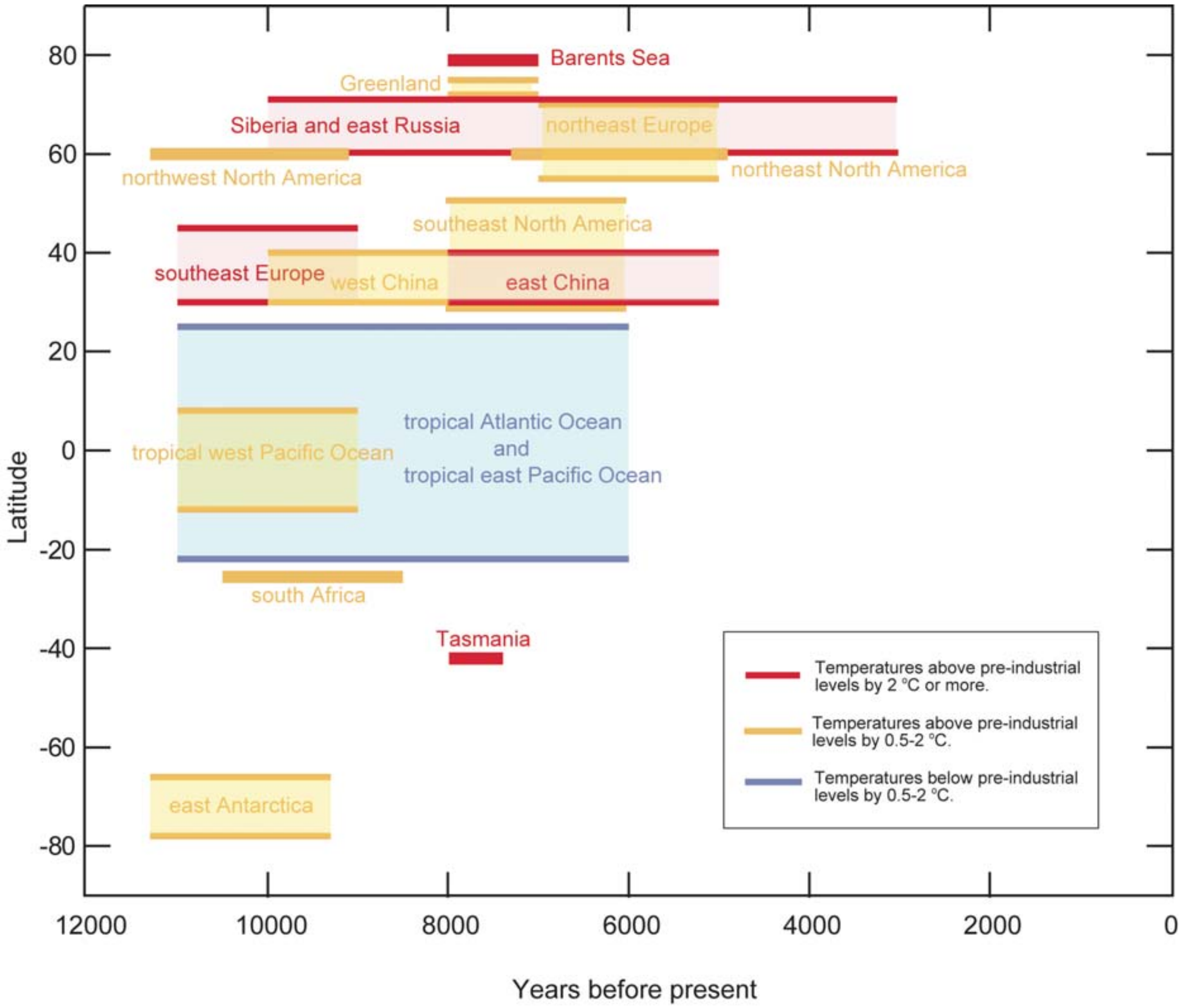

Figure 6.7. Timing and intensity of maximum multi-millenial temperature deviation from pre-industrial levels, as a function of latitude (vertical axis) and time (horizontal axis, in years before present). Temperatures above pre-industrial levels by 0.5°C to 2°C appear in orange (above 2°C in red). Temperatures below pre-industrial levels by 0.5°C to 2°C appear in blue. References for datasets are: Barents Sea (Duplessy et al., 2001), Greenland (Johnsen et al., 2001), Europe (Davis et al., 2003), Russia and Siberia (MacDonald et al., 2000) North America (Webb et al., 1998; Kaufman et al., 2004), China (He et al., 2004), tropical oceans (Rimbu et al., 2004; Stott et al., 2004), north Atlantic (Marchal et al., 2002), Tasmania (Xia et al., 2001), East Antarctica (Masson et al., 2000), Southern Africa (Holmgren et al., 2003).

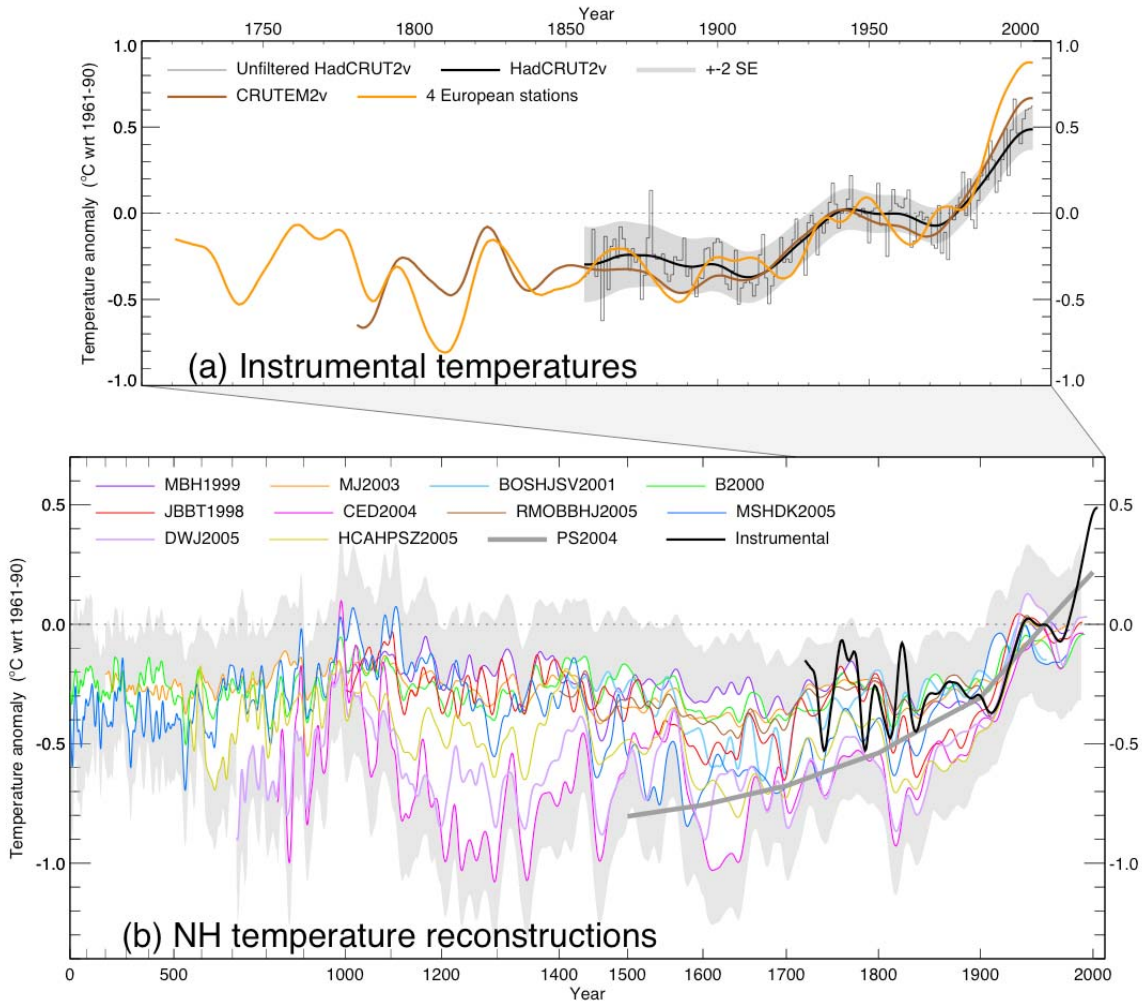

Figure 6.8. Records of Northern Hemisphere temperature variation during the last 2000 years.

(a) Annual-mean instrumental temperature records:
black = 1856–2004 HadCRUT2v land and marine temperatures for the full NH (Jones and Moberg, 2003), with ±2 standard errors shown by grey shading (Jones et al., 1997) and annual values shown by thin line;
brown = 1781–2004 CRUTEM2v land only temperatures for the NH only (Jones and Moberg, 2003; extended using data from Jones et al., 2003b);
orange = 1721–2003 average of temperatures from central England, de Bilt, Berlin and Uppsala in Europe.

(b) Reconstructions using multiple climate proxy records:
dark purple (MBH1999) = 1000–1980 annual land and marine temperatures for the full NH (Mann et al., 1999);
orange (MJ2003) = 200–1980 annual land and marine temperatures for the full NH (Mann and Jones, 2003);
light blue (BOSHJSV2001) = 1402–1960 warm-season land-only temperatures for the NH extra-tropics (Briffa et al., 2001);
green (B2000) = 1–1993 warm-season land-only temperatures for the NH extra-tropics (calibrated by Briffa and Osborn, 1999; Briffa, 2000);

red (JBBT1998) = 1000–1991 warm-season land-only temperatures for the NH extra-tropics (P. D. Jones et al., 1998; calibrated by Jones et al., 2001);
pink (CED2004) = 831–1992 annual land-only temperatures for the NH extra-tropics (Esper et al., 2002; recalibrated by Cook et al., 2004a);
brown (RMOBBHJ2005) = 1400–1960 annual land and marine temperatures for the full NH (Rutherford et al., 2005);
dark blue (MSHDK2005) = 1–1979 annual land and marine temperatures for the full NH (Moberg et al., 2005);
light purple (DWJ2005) = 713–1995 annual land-only temperatures for the NH extra-tropics (D'Arrigo et al., in preparation);
yellow (HCAHPSZ2005) = 558–1960 annual land-only temperatures for the NH extra-tropics (Hegerl et al., in preparation);
thick grey (PS2004) = annual NH extra-tropical temperatures estimated from ground boreholes (Pollack and Smerdon, 2004; reference level adjusted following Moberg et al., 2005);
black (Instrumental) = composite of the instrumental series shown in panel (a).

The grey shading is a purely indicative representation of reconstruction uncertainty typical of the group as a whole; the time-varying width of the shaded region is 1.5 times the average of the published standard errors of all individual reconstructions, applied either side of the envelope defined by the highest and lowest reconstructed values in any one year (the instrumental and borehole series are not used to define this envelope). Note that the *x*-axis time scale is deliberately non-linear to expand the time period when the number of series is greatest.

All series have been smoothed with a Gaussian-weighted filter to remove fluctuations on time scales less than 30 years; smoothed values are obtained up to both ends of each record by extending the records with the mean of the adjacent existing values. All temperatures represent anomalies (°C) from the 1961–1990 mean.

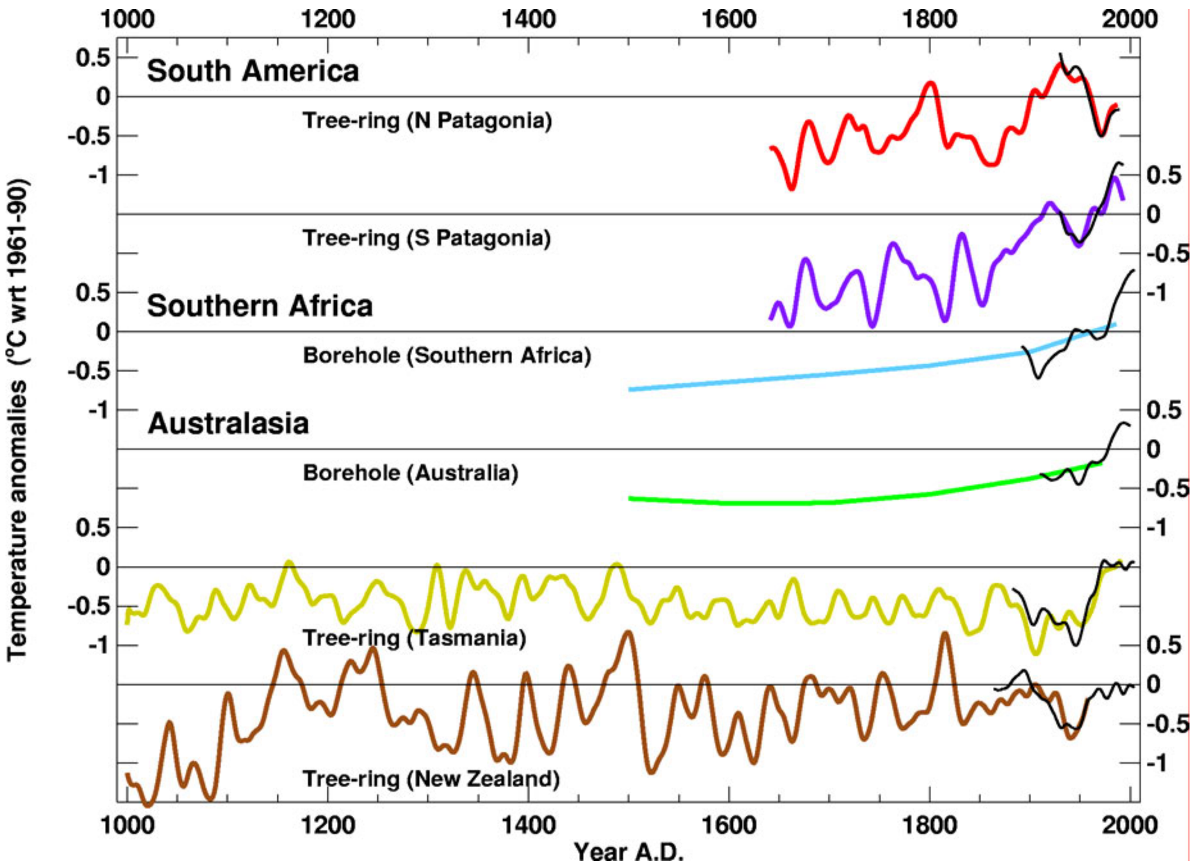

Figure 6.9. Temperature reconstructions for regions in the Southern Hemisphere: two annual temperature series from South American tree-ring data (Villalba et al., 2003); annual temperature estimates from borehole inversions for southern Africa and Australia (derived using the approach of Pollock and Smerdon (2004); summer temperature series from Tasmania and New Zealand tree-ring data (Cook et al., 2000; Cook et al., 2002). The black curves show summer or annual instrumental temperatures for each region. All tree-ring and instrumental series have been smoothed with a 25-year filter and represent anomalies (°C) from the 1961–1990 mean (indicated by the horizontal lines).

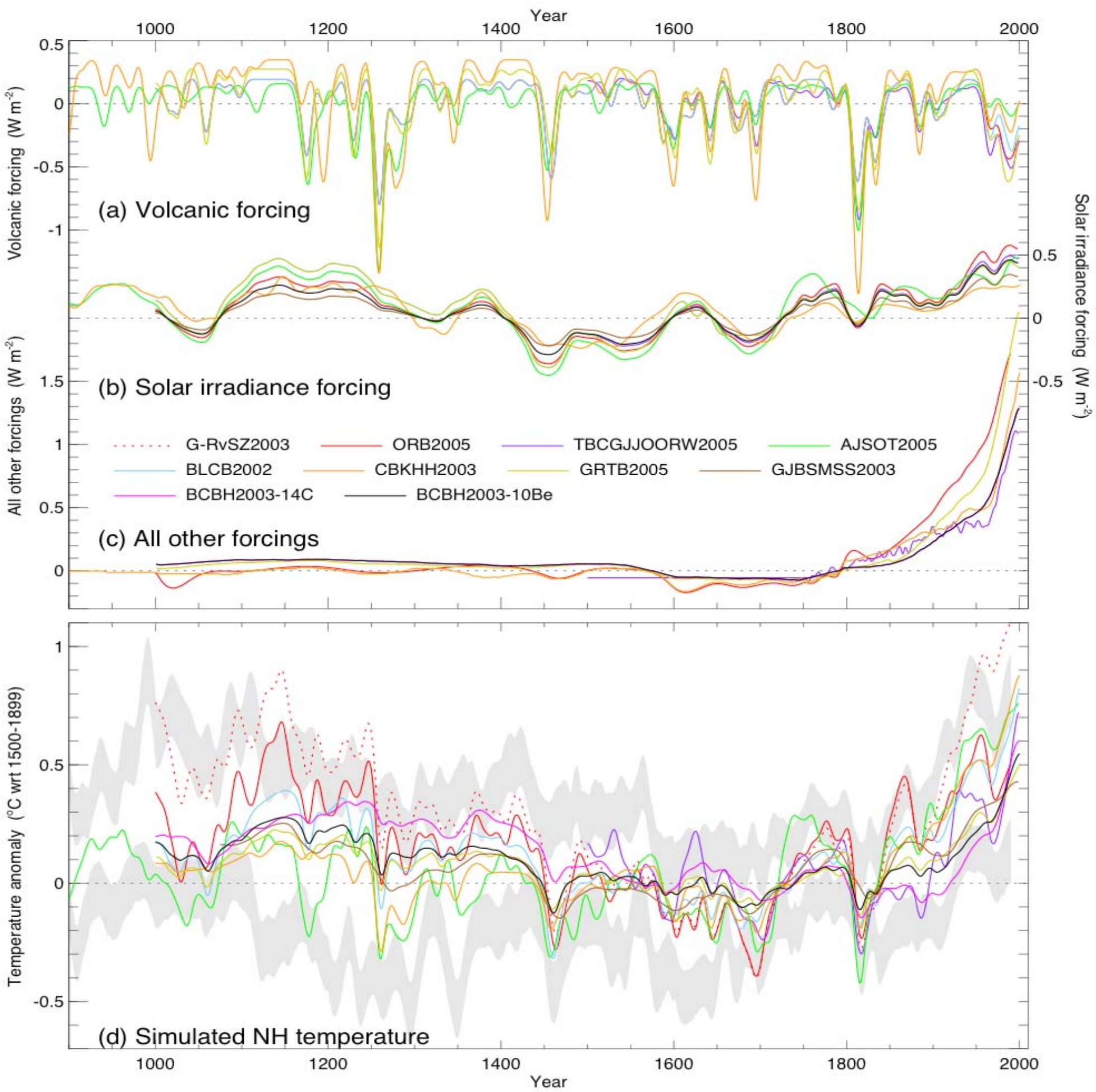

Figure 6.10. Radiative forcings and simulated temperatures during the last 1000 years.

Global-mean radiative forcing (W/m^2) prescribed to, or diagnosed from, climate model simulations due to (a) volcanic activity, (b) solar irradiance variations (these values are indicated by the labelling on the right-hand axis), and (c) all other forcings (which vary between models, but include greenhouse gases, tropospheric sulphate aerosols and land-use change). (d) Annual-mean NH temperature (°C) simulated by climate models. The envelope of reconstructed NH temperatures and indicative uncertainties (modified from Figure 6.5.1-1 to account for the 1500–1899 reference period used here) are indicated by the white region and the surrounding grey shading, respectively.

All forcings and temperatures are expressed as anomalies from their 1500–1899 means and then smoothed with a Gaussian-weighted filter to remove fluctuations on time scales less than 30 years; smoothed values are obtained up to both ends of each record by extending the records with the mean of the adjacent existing values.

The individual series are:

red dotted (G-RvSZ2003) = ECHO-G GCM (Gonzalez-Rouco et al., 2003; Von Storch et al., 2004);

red solid (ORB2005) = ECHO-G GCM adjusted for initial dis-equilibrium and to include tropospheric sulphate aerosols using a 1D EBM (Osborn et al., submitted);
purple (TBCGJJOORW2005) = HadCM3 GCM (Tett et al., submitted);
green (AJSOT2005) = NCAR CSM GCM;
blue (BLCB2002) = Louvain EMIC (Bertrand et al., 2002);
orange (CBKHH2003) = 3D EBM (Crowley et al., 2003);
yellow (GRTB2005) = ECBilt-CLIO EMIC;
brown (GJBSMSS2003) = EBM-based EMIC (Gerber et al., 2003a);
pink (BCBH2003-14C) and black (-10Be) = CLIMBER EMIC (Bauer et al., 2003) with solar irradiance forcing estimated using the ^{14}C record and the ^{10}Be record, respectively.

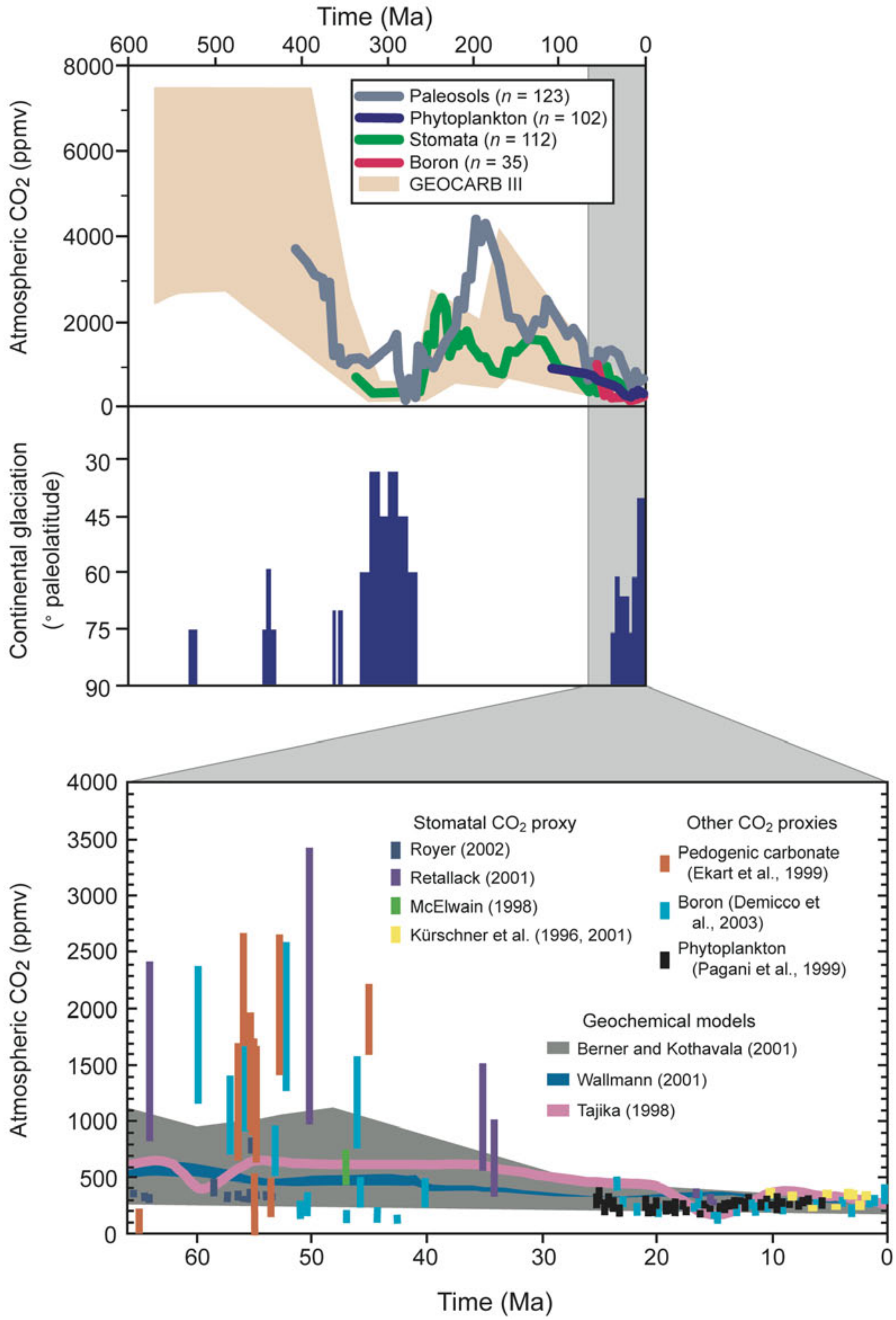

Box 6.1, Figure 1. Atmospheric CO_2 over 600 myr (top, shown with record of glaciation for the same period) and over the last 65 m yr (bottom). Five-point running averages of individual proxies for the last 600 MY, along with the range in error of GEOCARB III model also shown for comparison. The bottom diagram shows estimated CO_2 response for the time period covering the Pliocene and PETM in more detail. After Royer (2003).

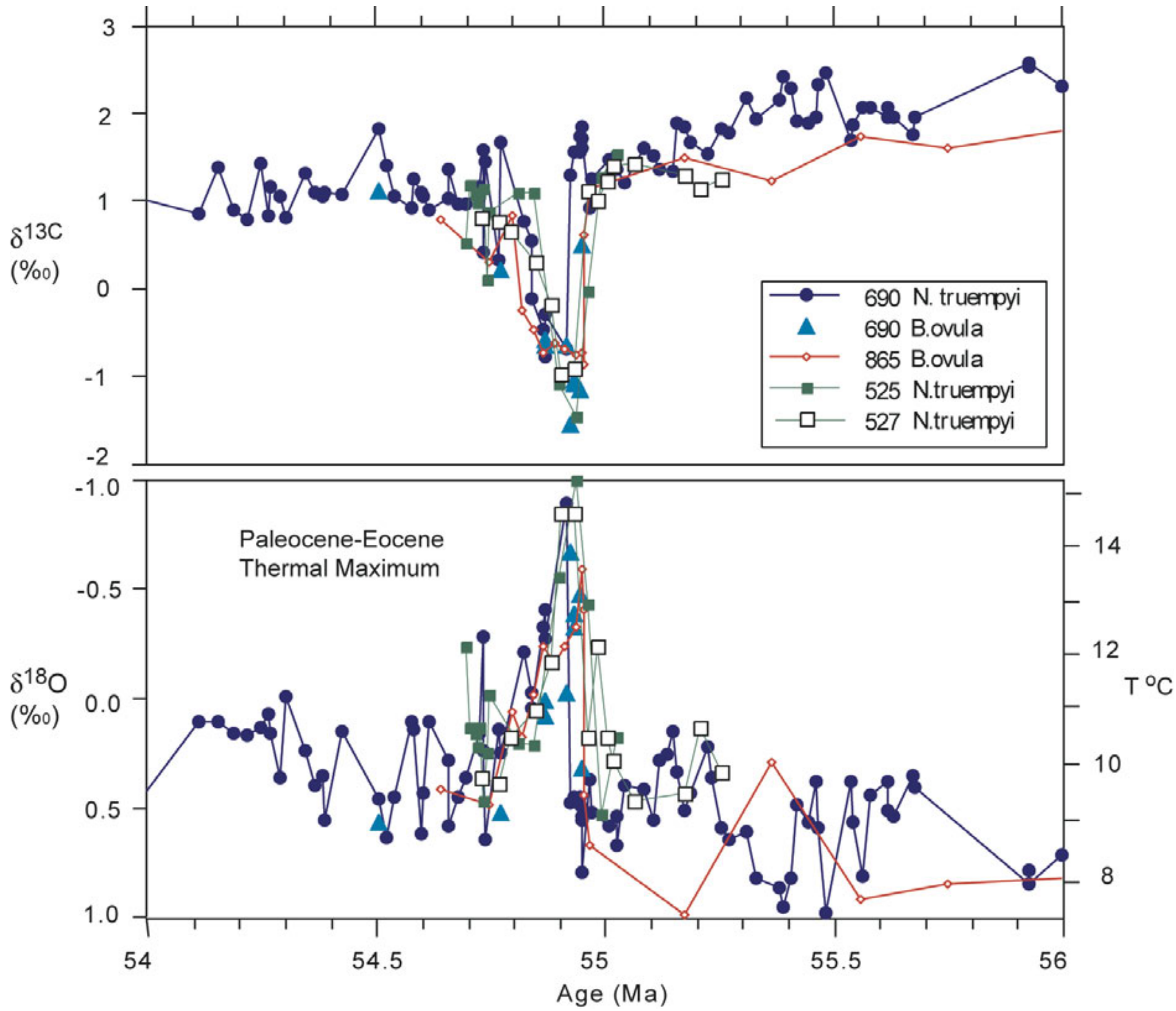

Box 6.1, Figure 2. The Paleocene-Eocene Thermal Maximum (PETM) as recorded in benthic isotopic records from sites in the south Atlantic and western Pacific (see Zachos et al., 2003 for details). The top panel provides strong evidence for a large increase in atmospheric greenhouse gases (CO_2 and/or CH_4), that was coincident with a major global warming event (bottom panel).

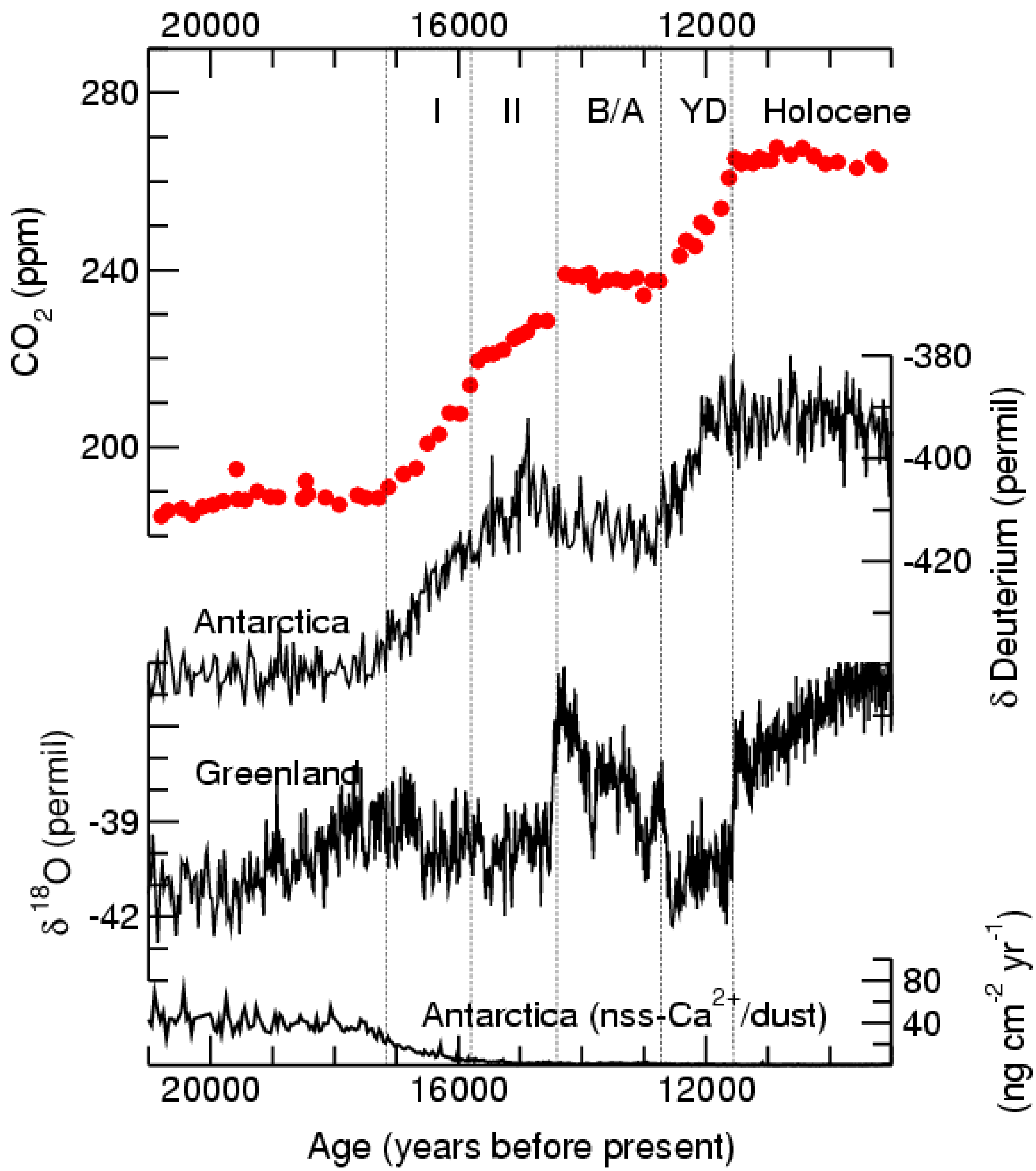

Box 6.2, Figure 1. The evolution of atmospheric CO_2 (red dots, top), local temperature in Antarctica (δDeuterium, middle) and Greenland ($\delta^{18}O$, bottom) (Monnin et al., 2001), and non-sea salt Calcium (a proxy for dust and iron deposition - Röthlisberger et al. (2004)). The records of atmospheric CO_2 and Antarctic temperature are highly correlated, and can be divided into four phases as indicated by dashed vertical lines. Temperature changes in Antarctica are smaller, and less abrupt, than in Greenland; temperature changes in Greenland and Antarctica are asynchronous. The B/A denotes the northern hemisphere Bølling/Allerød warm phase, and YD the northern hemisphere Younger Dryas cold phase (see text for more explanation). Measurements are from the EPICA ice core drilled at Dome Concordia, Antarctica, and from the GRIP ice core drilled at Summit, Greenland. The time scales of both cores have been synchronized to the GRIP scale.

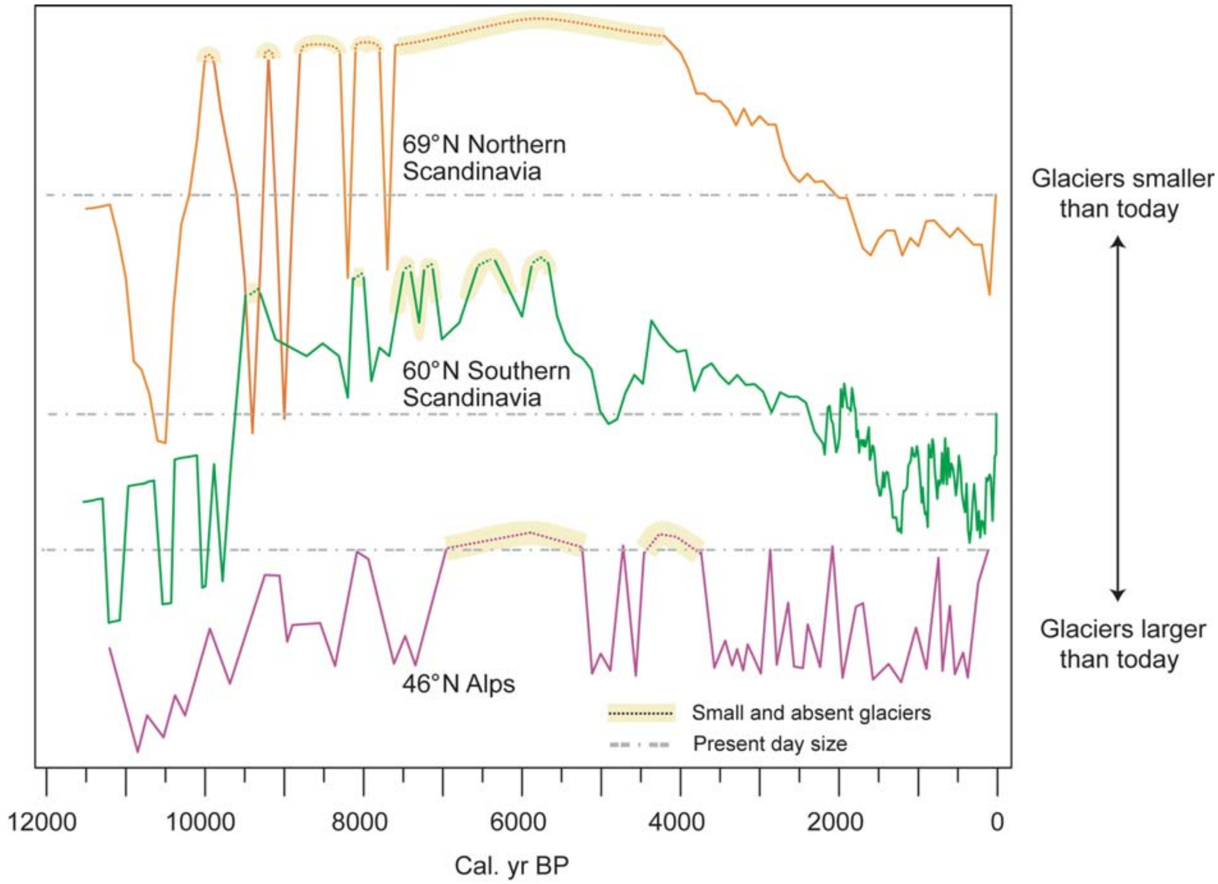

Box 6.3, Figure 1. Records of glacier size variations in Scandinavia and the Alps through the last 11,500 years. The data from Northern and Southern Scandinavia are based on continuous data sets retrieved from downstream glacier-fed lakes (Nesje et al., 2005 and references therein; Bakke et al., 2005a; Bakke et al., 2005b), whereas the data from the Alps are synthesized from a number of datasets (Holzhauser, 1998 and references therein).

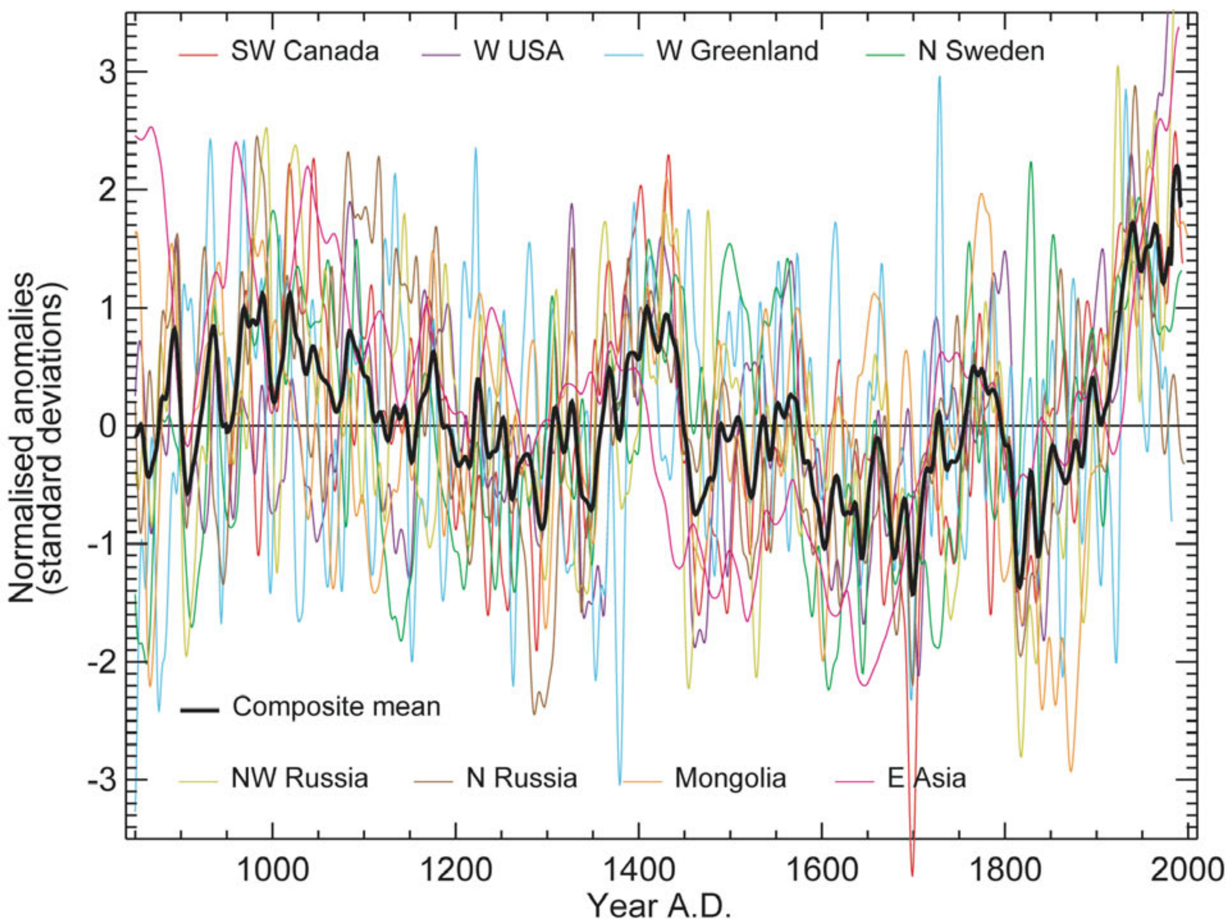

Box 6.4, Figure 1. The heterogeneous nature of climate during the Medieval Warm Period is illustrated by the wide spread of values exhibited by the individual records that have been used to reconstruct NH-mean temperature. The lines show individual, or small regional averages, of proxy records, selected from those used by Mann and Jones (2003), Esper et al. (2002) and (Luckman and Wilson, 2005), but excluding shorter series or those with an ambiguous relationship to local temperature. These records have not been calibrated (though all show positive correlations with local temperature observations), but have been smoothed with a 30-year filter and scaled to have zero mean and unit standard deviation over the period 1001–1980. The composite mean (black) indicates several periods of relative warmth (in the 11th, early 15th and late 20th centuries).